Proceedings of ASME Turbo Expo 2020
Turbomachinery Technical Conference and Exposition
GT2020
September 21-25, 2020, Virtual, Online

GT2020-14819

CFD-CRN STUDY OF NO_x FORMATION IN A HIGH-PRESSURE COMBUSTOR FIRED WITH LEAN PREMIXED CH_4 / H_2 - AIR MIXTURES

Ashish Vashishtha[1,*], Sajjad Yousefian[2,3,4,5], Graham Goldin[6], Karin Frojd[7], Sandeep Jella[8], Gilles Bourque[8], Rory F.D. Monaghan[2,3,4,5]

[1]Department of Aerospace, Mechanical and Electronic Engineering, Institute of Technology, Carlow, IRELAND R93 V960
[2]School of Engineering, National University of Ireland, Galway, IRELAND H91 TK33
[3]Combustion Chemistry Centre, National University of Ireland, Galway, IRELAND H91 TK33
[4]Ryan Institute, National University of Ireland, Galway, IRELAND H91 TK33
[5]MaREI Research Center for Marine and Renewable Energy, Galway, IRELAND H91 TK33
[6]Siemens CD-Adapco, Lebanon, NH, USA 03756
[7]Siemens PLM Software, Skane, SWEDEN
[8]Siemens Canada Ltd., 9545 Cote de Liesse Road, Montreal QC H9P 1A5, CANADA

ABSTRACT

The main motivation of this study is to investigate detailed NO_x and CO formation in high-pressure dump combustor fired with lean premixed methane-air mixture using CFD-CRN hybrid approach. Further, this study is extended to investigate the effect of H_2 enrichment on emission formation in the same combustor. Three-dimensional steady RANS CFD simulations have been performed using a Flamelet Generated Manifold (FGM) model in Simcenter STAR-CCM+ 2019.2 with the DRM22 reduced mechanism. The CFD simulations have been modelled along with all three heat transfers modes: conduction, convection and radiation. The conjugate heat transfer (CHT) approach and participating media radiation modelling have been used here. Initially, CFD simulations are performed for five lean equivalence ratios ($\phi = 0.43$-0.55, $T_{inlet} = 673$ K, $V_{inlet} = 40$ m/s) of pure methane-air mixture operating at 5 bar. The exit temperature and flame-length are compared with available experimental data. The automatic chemical reactor network has been constructed from CFD data and solved using the recently developed reactor network module of Simcenter STAR-CCM+ 2019.2 in a single framework for each cases. It is found out that the CRNs up to 10,000 PSRs can provide adequate accuracy in exit NO_x predictions compared to experiments for pure methane cases. The contribution of NO_x formation pathway, changes from N_2O intermediate to thermal NO as equivalence ratio increases. Further studies are performed for two equivalence ratios ($\phi = 0.43$ and 0.50 to simulate the impact of H_2 addition (up to 40% by volume) on NO_x formation pathways and CO emission. It is found out here that the contribution from NNH pathway increases for leaner equivalence ratio cases ($\phi = 0.43$), while thermal pathway slightly increases for $\phi = 0.50$ with increase in H_2 content from 0% to 40%.

Keywords: Emissions, H_2-Enriched, Lean Premixed, Reactor Network, NO_x Pathways

1. INTRODUCTION

Emission estimations by using numerical methods or tools are important requirements for the design, development and performance analysis of future gas turbine combustors. Furthermore, the prediction of pollutants that constitute a few ppm, requires use of detailed chemical kinetic mechanism in numerical simulations. Using a detailed chemical kinetic mechanism with the complex geometry and large size domain of an industrial burner incurs large computational cost. Hence, many researchers as outlined in review paper [1], have used hybrid computational fluid dynamics (CFD) and chemical reactor network (CRN) approaches to estimate pollutants in various turbulent flames. This hybrid approach have been first proposed and used by Ehrhardt [2, 3]. In this approach, it is required to use the CFD simulations for mean flow field and major species in the combustor in order to construct a chemical reactor network (CRN). The integration of detailed chemical kinetic mechanism in chemical reactor network is performed to solve CRNs for emission estimation [4, 5]. The traditional hybrid CFD-CRN methods [1] have two kinds of limitations: 1) construction of the reactor network model is based on user experience and skills in order to divide the flow field into difference PSRs (perfectly stirred reactors) and PFRs (plug flow reactors), 2) solving large size of reactor network with detailed chemical kinetics requires higher computational resources.

*Corresponding author: vashish.aero@gmail.com

The exit emissions in many simple combustors are estimated by simply solving fewer than 100 reactors in a CRN in many studies [1]. However, in order to study the formation of emissions in the various regions inside industrial combustors as well as chemical formation pathways, it may be required to use a systematic approach for construction of large reactor network (sizes O ($10^3 \sim 10^6$)) from CFD data. As well as this, the quick solution of CRNs can also facilitate the process of uncertainty quantification and probabilistic modelling that requires a large number of simulations [6, 7]. Some approaches [8] have used homogeneous zones, based on intervals of important flow parameters (Temperature, mixture fraction, velocity) to construct the reactor network. Further, the size of reactor network is limited by the use of a detailed kinetic mechanism and the capability of the solver to handle a large number of equations for each reactor in the network. As recently reviewed by Yousefian et al. [1], only KPP [9] and KPP-Smoke [10] (excluding currently used STAR-CCM+ 2019.2) are able to solve large number of reactor networks [4, 5] among various CRN solvers. In the qualitative assessment of various CRN solver [1], most of the hybrid CFD-CRN methods use different CFD and CRN frameworks, which may require additional set-up time to construct CRN from CFD data. Currently, CFD-CRN capabilities are being developed in Simcenter STAR-CCM+ version 2019.2 [11] onward. The single framework of STAR-CCM+ can be used for (1) CFD simulation, (2) reactor network construction, (3) CRN solution and (4) graphical post-processing of parameters. It overcomes the difficulties of traditional CFD-CRN limitations as mentioned above. This study aims to utilize the hybrid CFD-CRN approach in Simcenter STAR-CCM+ to estimate detailed NO_x and CO formation in a lean premixed pure methane - air flame as well as H_2 enriched methane - air flame in a high-pressure combustor (Paul Scherrer Institute (PSI) burner [12–14]).

Lean premixed combustion is an established technology for stationary gas turbines fueled by natural gas to achieve lower emissions and higher efficiency. However, due to growing concern over climate change and the effects of pollutants on human health, more stringent emission regulations are expected in future. It is required to optimize the combustor system for further lower emissions than current level. NO_x and CO are two main regulated pollutants for stationary gas turbines [15] and reliable predictions of their formation in the combustor and mitigations are important for future design and development of gas turbine engines. Blending the fuel with hydrogen or other hydrocarbon fuels is also one of the promising techniques to increase the lean blowout limit and may reduce or keep the emissions at same level [12]. Boschek et al. [12] have experimentally studied the effects of adding hydrogen and propane to methane for increasing the lean blowout limit and reducing NO_x emission in a dump combustor. Griebel et al. [13] have studied piloted and perfectly premixed H_2 addition effects on LBO and NO_x emissions. In this study, test cases performed by Gribel [12, 13] with perfectly premixed H_2 addition up to 40% by volume at two lean equivalence ratios are investigated along with pure methane-air cases for NO_x and CO emissions using Simcenter STAR-CCM+ 2019.2 [9].

Taamallah et al. [16] have reviewed fuel flexibility and emission trends of using hydrogen blends in natural gas fired as well as syn-gas fired premixed combustors. In a premixed methane-air mixture, blending hydrogen modifies the characteristics of flames such as adiabatic flame temperature and laminar / turbulent burning velocity, auto-ignition characteristics. Because of the change in flame characteristics, peak temperature and temperature distribution might get affected, which can lead to different NO_x formation pathways than the pure methane-air mixture. Rajpara et al. [17] have investigated the effect of hydrogen addition on combustion and emission in upward swirl can combustor fueled with methane. It was found out that at constant heat input condition, increase in hydrogen content up to 10% by mass leads to increase in NO_x level because of higher flame temperature, while at constant volumetric conditions, increase in hydrogen content up to 80% by volume leads to reduction in CO emissions with marginal increase in NO_x. Recently de Persis et al. [18] have experimentally studied the effect of hydrogen addition in high pressure counter flow premixed CH_4/air flames for the pressure ranging from 0.1 MPa to 0.7 MPa with 20% hydrogen substituted to CH_4 by volume. It is found that with increase in pressure, the peak NO_x increases. The kinetic analysis shows that there is increase in thermal NO pathways at high pressures with hydrogen addition while N_2O pathway contribution decreases. From many previous studies, it can be said that hydrogen addition will lead to increase in flame temperature, which may increase NO_x emission, but the kinetic pathway for NO_x formation may depend on combustor sizing and operating conditions etc.

In this study, the operating conditions of test cases [12] are selected close to lean blow-out limit of methane-air mixture. The NO_x emissions at the exit for tested case are less than 2 ppmv (15% dry O_2) up to $\phi = 0.53$ for pure methane-air mixture. Accurately predicting NO_x emission of this small range is challenging without proper heat transfer modelling. To summarize the whole paper, the mean flow field from CFD simulation (with heat transfer modelling) of a high pressure dump combustor are computed by using the Flamelet Generated Manifold (FGM) model in Simcenter STAR-CCM+ 2019.2. The construction and solution of the reactor network have been performed in the same framework. The advantages of reactor network in Simcenter STAR-CCM+ are that it uses clustering algorithm for automatic reactor network creation in the same framework using the CFD data and it utilizes variable time-stepping and efficient ODE integration of CVODE solver [19] for large number of equations in the CRN solver. These advantages leads to significant reduction in time for reactor network construction and solution. The main objectives of this study are as follows: (1) CFD-CRN study for the PSI dump combustor operating at lean conditions for pure methane-air as well as hydrogen enriched methane-air premixed flame, (2) Investigate the effects of equivalence ratio as well as hydrogen addition on NO_x formation pathways.

2. DESCRIPTION OF TEST-CASE

The PSI burner [12–14] consists of a high-pressure combustor of inner liner cross-section diameter of 75 mm as shown Fig. 1a. The preheated methane-air premixed mixture flows through a 25 mm diameter inlet pipe. In the experimental rig, preheating to 673-873 K has been performed using an electric heater. A perforated turbulence grid is placed in the inlet pipe to increase

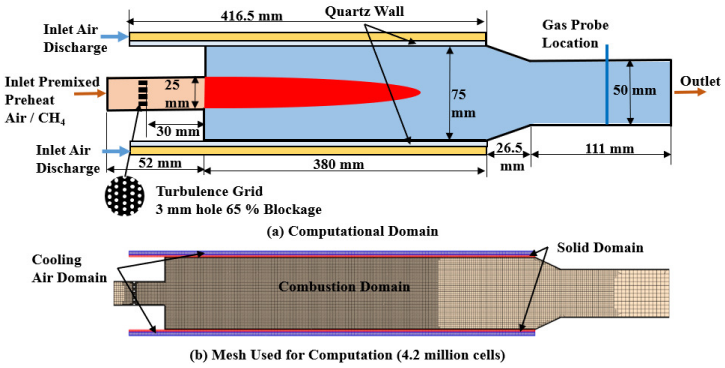

FIGURE 1: (A) DESCRIPTION OF TEST-CASE AND COMPUTATIONAL DOMAIN (B) MESH USED FOR COMPUTATION

the turbulence in the flow field [13]. The current study focuses on test cases based on one turbulence grid, g365 × g10, which means 3 mm holes are placed to give 65% blockage of cross section area of inlet, located at 10 times the diameter of holes from the inlet plane of the dump combustor. In the PSI dump combustor, flame stabilization occurs because of re-circulation of flue gases in the sudden expansion zone. The experimental combustor had optical access, which has been used for PIV measurements in non-reacting cases [13] and OH-LIF, CH_2O-LIF measurements for reacting cases. Major species (CO_2 and O_2) as well as NO_x and CO are measured at the combustor exit by a water-cooled gas probe connected to an exhaust gas analyzer. The exhaust gas temperature has also been measured at the combustor exit using a thermocouple. The measured temperatures are corrected for heat losses due to radiation, convection and conduction from thermocouple according to Siewert [14]. OH-LIF images are used to locate the flame front from the image processing of time-averaged images, as described by Griebel et al. [20].

This study simulates test cases for pure methane-air mixture at the following conditions: preheat temperature of 673K, lean premixed methane-air mixture of equivalence ratio ϕ=0.43, 0.46, 0.50, 0.53 and 0.55, inlet velocity of 40 m/s, and operating pressure of 5 bar. Further, 10% to 40% of H_2 enrichment at lean equivalence ratio ϕ=0.43 and intermediate equivalence ratio ϕ=0.50 have also been studied. The flame front location and corrected exit temperature, NO_x and CO measured values are used to validate CFD and analyze CFD-CRN results. The exit NO_x at these low equivalence ratios are under 2 ppm (15% dry O_2) [13] up to equivalence ratios 0.53. The distribution of NO_x formation inside the combustor is expected to be highly affected by heat transfer distribution from the wall of the combustor. The assumptions of adiabatic wall or isothermal wall are not sufficient to predict the detailed emissions formation correctly using CFD or CFD-CRN in this low range of under 2 ppmv. Hence the realistic heat transfer modelling is important at these low equivalence ratios. The combustor in experimental test-rig is cooled by convective air discharged through the double walled quartz tubes as shown in Fig. 1a. Other heat transfer modes prevalent in the test-rig are conduction through the quartz walls and radiation from the high temperature flame and reaction products. Hence, the conjugate heat transfer approach with radiation heat transfer modelling have been utilized in the CFD simulations by simulating multiple solid and fluid domains as shown in Fig. 1b.

3. CFD-CRN METHODOLOGY

Steady three-dimensional CFD with conjugate heat transfer approach and radiation modelling is performed for various operating conditions, using Simcenter STAR-CCM+ 2019.2 [11]. Later, CRN modelling has also been performed in the same framework. Figure 1a shows the domain used for CFD simulations, with a 25 mm diameter inlet containing g365 × g10 turbulence grid. The dump combustor has diameter of 75 mm, length of 380 mm and an outlet pipe of 50 mm. The exit emission and temperatures are calculated at center of plane located axially 450 mm from the combustor inlet, the same location used in experiments by Boscheck et al. [12]. As mentioned earlier, the whole computation domain consists of the main combustion domain, quartz wall solid domain and fluid domain for cooling air in an annular passage. The second quartz wall is not modelled, and the inner layer of outer quartz wall is assumed isothermal at the same temperature as cooling air.

3.1 Combustion Modelling

In all CFD cases, combustion modelling is performed using the tabulated chemistry approach with the non-adiabatic Flamelet Generated Manifold (FGM) model in Simcenter STAR-CCM+ by using DRM22 [21], reduced chemical kinetic mechanism. The flame regime of the studied operating conditions, fall in the thin reaction zone regime, because of highly stretched and highly turbulent flames [14], hence the choice of FGM modelling is appropriate. The FGM model in Simcenter STAR-CCM+ requires generation of a five-dimensional pre-calculated FGM table in mixture-fraction, unnormalized progress variable, their variances, and heat loss ratio. In the current study, FGM model is implemented using a 1D premixed counter-flow flamelet configuration to account for the flame strain effects. The progress variable is defined based on equal weights of mass fraction of CO and CO_2. The variance of progress variable is modelled using a transport equation. Along with reactant and complete combustion product species, intermediate species CO, O, CH_2O and OH are tabulated in the FGM model. Thermal NO is also modelled in the CFD simulations, where NO_x chemistry is decoupled from the flow and combustion simulation, and is solved by a transport equation for NO_x with a thermal NO source term. The thermal NO source term is based on extended Zel'dovich mechanism and has been calculated using four coefficients, which are stored in FGM table [11]. Although Simcenter STAR-CCM+ uses adaptive generation of FGM table, three different sizes of final FGM tables are tested for equivalence ratio ϕ = 0.5, and it is found that exit temperature does not vary more than 0.1%, while flame length can vary up to 5%, while using different FGM table sizes. Finally, FGM table with size as $13 \times 72 \times 22 \times 51 \times 5$ is used for all the calculations for heat loss, mixture fraction and its variance, progress variable and its variance, respectively. In order to model combustion for H_2-enriched methane-air mixture, different FGM tables have been generated for different volumetric contents of H_2 in CH_4 using 1D premixed counter-flow flamelet.

However, FGM tables are not changed for studying two different equivalence ratios, $\phi = 0.43$ and 0.50 for each content of H_2.

The multicomponent gas flow is modelled using the segregated flow solver with the compressible ideal gas model, which uses the SIMPLE type algorithm for pressure velocity coupling [11]. The RANS Realizable $k - \epsilon$ model is used for turbulence modelling. Dinkelacker et al. [22] have studied the same PSI combustor for various H_2 concentration in premixed mixture at various pressure level and concluded that the assumption of unity Lewis number does not hold for modelling high-pressure turbulent flames. Hence, in this study, mean molecular diffusivity and thermal conductivity and dynamic viscosity have been modelled as mixture averaged quantities based on flamelet species and temperature with adjusted Turbulent Schmidt number (S_{cT} =) 0.6 for flame length. As hydrogen molecular diffusivity is higher than methane, hence for increased hydrogen contents in mixture, turbulent Schmidt number has been further adjusted, which is discussed in results section. In all the simulated cases, the operating pressure in the combustion domain is absolute 0.5 MPa. At the inlet, a velocity inlet (40 m/s) boundary condition is used and zero gradient boundary condition is used for all the variables at outlet. The inner wall of quartz combustor tube is defined as the interface with solid domain and energy transfer is modelled with conjugate heat transfer.

3.2 Heat Transfer Modelling

Lyra et al. [23] have studied the same combustor with adiabatic wall boundary assumptions, comparing the exit NO_x and CO for three equivalence ratios and found 500 PSRs are sufficient to compare against available experimental data. In the above study, the exit NO_x for two equivalence ratios ($\phi = 0.43$ and 0.50) were predicted well with 500 PSRs. The detailed NO_x formation studies may require higher number of PSRs with accurate temperature distribution in whole combustor. In order to have accurate prediction of temperature distribution in combustor, conduction, convection and radiation heat transfer are modelled in this study. The solid domain attached to the combustion domain (in Fig. 1a) is modelled as a quartz wall by solving the energy balance equation. The density for the quartz wall was set to be constant (2200 kg/m^3). The specific heat and thermal conductivity for quartz wall have been assigned as polynomial functions according to Sergeev et al. [24]. Although the polynomial for heat conductivity of quartz is available up to 800 K, the same polynomial has been used for higher temperature in this study assuming that there will be not much variation in heat conductivity at higher temperature. The convective heat transfer is modelled with a second fluid domain (as shown in Fig. 1), which consists of air discharged in the annular passage between the double wall quartz tubes. The inner wall of outer quartz cylinder attached to this fluid domain is modelled as isothermal wall of 673 K. The second quartz wall is not modelled as solid. The radiation is modelled with the participating media radiation model with the optically thin flame assumption. Planck mean absorption coefficients for species CH_4, CO_2, CO and H_2O have been modelled as polynomials in temperature and the coefficients are accessed from [25].

The data for heat loss for all the operating cases as well as the fraction of discharge air passing through the annular passage are not available in open literature. For the 5 bar operating condition, only for equivalence ratio 0.5, the total heat loss data is available in Chapter 4 of [14] as 8 $\sim$ 12%. Several trials have been made to estimate discharge air passing through the annular passage in order to achieve the heat loss from the combustor wall as predicted in the experiments. It was found that 40 - 50% of the total mass flow rate used in air discharge leads to correct predictions of exit temperature and flame length compared to experimental predictions. For all the cases studied in this work, 40% discharge air fraction has been used for cooling air, while 50% has been used only for higher equivalence ratios $\phi = 0.53$ and 0.55, where it may be possibly required to have higher cooling because of high flame temperatures in higher equivalence ratios mixtures.

Figure 1b shows the hexahedral computational mesh, which was generated in Simcenter STAR-CCM+ 2019.2 with the cut-cell method for all three domains with 5 prism layers near the wall boundary and at interfaces. The mesh shown in Fig. 1b has 1 mm cell size in the flame zone, while the turbulence grid is discretized with 0.5 mm cells. The entire domain consists of approximately 4.2 million cells. To perform a grid independence study, one coarse grid with 2 mm cell size in the flame zone (approx. 2.8 million cells) and one fine grid with 0.5 mm cell size in the flame zone (approx. 6.8 million) are also simulated for equivalence ratio case (ϕ=0.5). Between medium (4.2 million) and fine (6.8 million) mesh, there are no significant differences in exit temperature predictions (less than 1%) and flame front location (less than 5%). However, flame front location can be adjusted by Turbulent Schmidt number. In the current study, the medium mesh with 4.2 million grid size is used for all the cases.

3.3 CRN Modelling

After achieving a steady state solution for converged CFD results, chemical reactor network (CRN) studies are performed in Simcenter STAR-CCM+ 2019.2. The process involves automatic creation of a network of reactors, which are based on clusters of CFD cells with selected homogeneous parameter intervals of temperature, mixture fraction of reactants, products and intermediate species, equivalence ratio, and solving the 0-D reactor network using detailed chemistry. In the current study, the GRI 3.0 mechanism [21] has been used for solving reactor networks. The clustering algorithm for creating the reactor network requires inputs such as interval of clustering parameter, total number of reactors in the network. The user chooses single or multiple predefined or user-defined parameters for clustering and can provide the finite interval for them. The clustering algorithm is based on three steps. In the first step, a multi-dimensional table is created based on the clustering parameters and their intervals e.g. the target number of PSRs to create reactor-network is given 2000 and there are three parameters velocity, equivalence ratio and temperature are selected for clustering with 20 intervals in each parameters, the multi-dimensional table will be generated of size $20 \times 20 \times 20$ or 8000. The CFD cells are then given indexes or grouped based on the interval of clustering parameter in this multi-dimensional table of 8000 indices. In the next step, the non-connected cell clusters are split into different clusters. The

third step is called agglomeration, in which the small cell clusters are merged with their neighbours to achieve the required number of clusters or reactors (in the above example 2000 PSRs).

There are two types of reactor available for solving the reactor network: constant pressure reactors and perfectly stirred reactors (PSRs). In this study, the reactor networks are solved using PSRs. After creation of a reactor network, in each PSR, the convection and diffusion mass fluxes $\dot{m}_{ij}$ are calculated from the cell face fluxes to and from neighbouring reactors, here $\dot{m}_{ij}$ denotes the mass flux into reactor i from reactor j. Species mass sources are calculated from boundary inlets or any volumetric mass source, and denoted as S_k^i for the reactor i and species k. The mass in reactor i is denoted as m_i and reaction rate for the reactor i and species k is donated as $\dot{r}_k^i$ The total mass flow into a reactor can be defined as:

$$\dot{m}_i = \sum_{j=1, j\neq i}^{N} \dot{m}_{ij} + \sum_{k=1}^{K} S_k^i \tag{1}$$

Here, N is total number of reactors and K is total number of species. The PSR species conservation equation for reactor i is:

$$\sum_{j=1, j\neq i}^{N} \dot{m}_{ij} Y_k^j - \dot{m}_i Y_k^i = \dot{m}_i \dot{r}_k^i + S_k^i \tag{2}$$

where, Y_k^i is species k mass fraction in reactor i. In the limit of single reactor, the standard PSR equation is obtained as:

$$\frac{Y_k^{in} - Y_k}{\tau} = \dot{r}_k \tag{3}$$

where τ is the residence time in the single reactor, defined as ratio of total mass in the reactor and mass flow rate. The energy equation is not solved in the current CRN solver. As the mass and volume of each reactor is constant and pressure is constant, the temperature of each reactor is calculated using the equation of state. The system of equations for the reactor network are solved using the efficient integrator and fast CVODE ODE Solver [19] in Simcenter STAR-CCM+, which solves the large number of reactors with lower computational cost.

4. RESULTS & DISCUSSION

The results are discussed in three subsections. In the first subsection, the results obtained from CFD simulations with heat transfer and radiation modelling have been discussed for studied lean equivalence ratios of pure methane-air mixture as well as the effect of H_2 addition up to 40% by volume for two equivalence ratios $\phi = 0.43, 0.50$. As it was mentioned earlier, CFD data have been used as basis for creating chemical reactor network and computing the mass fluxes in each reactor, hence it is important to predict the the exit temperature and flame length in combustor as close to experimental measurements. In the second subsection, CFD-CRN results with respect to reactor network size independence and estimated exit NO_x and CO for all the cases have been discussed. Finally NO_x pathway analysis have been performed to study the effect of equivalence ratio as well as H_2 addition in the last subsection.

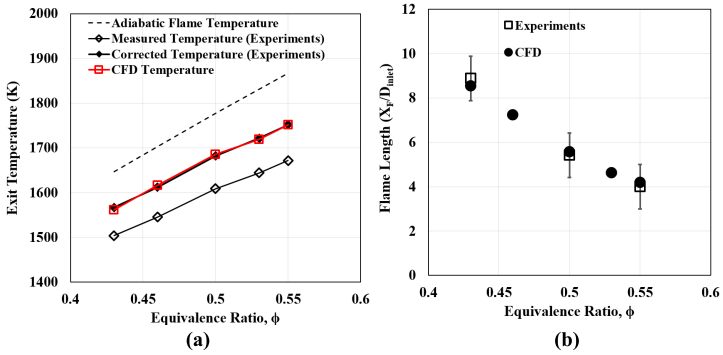

FIGURE 2: (A) EXIT TEMPERATURE (B) NON-DIMENSIONAL FLAME FRONT LOCATION FOR PURE METHANE-AIR MIXTURE

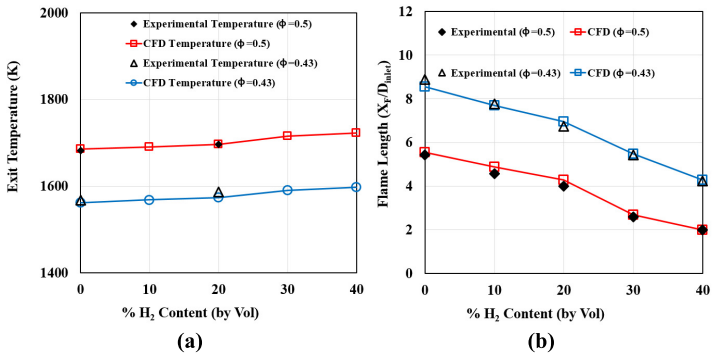

FIGURE 3: EFFECT OF H_2 ADDITION ON (A) EXIT TEMPERATURE (B) NON-DIMENSIONAL FLAME FRONT LOCATION FOR METHANE-AIR MIXTURE

4.1 CFD Results

Figure 2a shows the comparison between calculated exit temperature from CFD simulations and measured exit temperature for various equivalence ratio changing from 0.43 to 0.55 of 100% methane-air premixed mixture. In the experiments, [12] the exit temperatures are measured at the center of exit plane located at 450 mm from combustor inlet. Further, the measured temperatures are corrected for heat loss due to conduction, convection and radiation from the thermocouple according to method given in appendix of [14]. The corrected temperatures are approximately 60K ~ 70K higher than the measured values. The predicted temperatures from CFD results are compared with the corrected temperatures. Adiabatic flame temperatures for each equivalence ratios are also plotted, which gives indication of heat losses through the combustor wall and radiation. For $\phi = 0.43$, 0.46 and 0.50, the exit temperature vary linearly along with adiabatic flame temperature but for higher equivalence ratios for pure methane there are slightly higher heat losses through combustor and the exit temperature slightly deviates from linearity. It should be noted that the air discharge in the annular passage has been kept constant at 40% fraction for $\phi = 0.43$, 0.46 and 0.5, while it needs to increase to 50% for higher equivalence ratios for $\phi =$ 0.53 and 0.55 in order to accommodate the higher heat losses. The experimental data [14] for relative heat loss (Q_{loss}/Q_{load})

from the combustor is available only for ϕ = 0.50 at 5 bar as 8% ~ 12%. It is observed that computed radiation relative losses from CFD in all the examined cases are in range of 2% ~ 4% and can cause reduction in exit temperature up to 20K ~ 30K. Also, the radiation losses are from the flame surface, hence it was important to model radiation to predict temperature distribution in the combustor.

Figure 2b shows a comparison between the non-dimensional axial flame front location for different equivalence ratios of pure methane-air premixed mixture. The flame front is defined as the inflection point on OH mass fraction plotted along the axis of the combustor. There is no significant difference between experiments and CFD flame front location for all the equivalence ratio of pure methane-air premixed mixture. The flame length is higher for lower equivalence ratio, while it decreases linearly with increase in equivalence ratio. In combustion modelling, the flame length can be adjusted with change in turbulent Schmidt number (S_{cT}), however it has been kept constant for all the pure methane-air as 0.60. Table 1 shows the turbulent Schmidt number (S_{cT}) and discharge air fraction for cooling air used for different cases in this study. These two parameters (cooling air discharge fraction and Turbulence Schmidt numbers) can be effectively used as controlling parameter for exit temperature prediction and flame front location in the current study.

Figure 3 plots the computed exit temperature as well as non-dimensional flame front location from CFD simulations related to H_2 addition up to 40% by volume for two equivalence ratios ϕ = 0.43 and 0.50 along with experimental results. The experimental exit temperatures in Fig. 3a, are plotted as corrected temperature for 0 and 20% H_2 addition. The computed exit temperature from CFD matches with experimental corrected temperature. As the H_2 content increases, there is a slight increase in exit temperature about 5 K for each 10% increase at both equivalence ratios. The non-dimensional flame length (in Fig. 3b) decreases linearly, with increase in H_2 content for both equivalence ratio. The H_2 is more diffusive and reactive than methane and increase in its content in mixture may lead to increase in flame temperature as well as increase in flame speed, which causes reduction in flame length. In the current study, unity Lewis Number assumption have not been used and molecular diffusivity and thermal conductivity have been modelled as mixture averaged quantities in Flamelet table. However, it was required to reduce turbulent Schmidt number (S_{cT}) in order to predict comparable flame length with experimental data for 30% and 40% H_2 addition at both equivalence ratios. The reason for changing turbulent Schmidt number is that the mixture averaged properties (dynamic viscosity) may not be the effective estimation for higher content of hydrogen in mixture. The turbulent Schmidt number has been adjusted to 0.3 for 40% H_2 addition at both ϕ = 0.43 and 0.50, while 0.35 and 0.50 for 30% H_2 addition at ϕ = 0.43 and 0.50, respectively. The temperature contours are compared and discussed between CFD and CFD-CRN in later section.

4.2 CFD-CRN Results

After achieving steady CFD results with satisfactory accuracy in temperature distribution and flame length, automatic reactor network construction and simulations are performed in

TABLE 1: PARAMETERS FOR CFD-CHT STUDY

ϕ	%CH_4:%H_2	turbulent Schmidt Number (S_{cT})	Fraction of Discharge Air for cooling
0.43 - 0.50	100:0	0.60	40%
0.53 and 0.55	100:0	0.60	50%
0.43	90:10	0.60	40%
	80:20	0.60	40%
	70:30	0.35	40%
	60:40	0.30	40%
0.50	90:10	0.60	40%
	80:20	0.60	40%
	70:30	0.50	40%
	60:40	0.30	40%

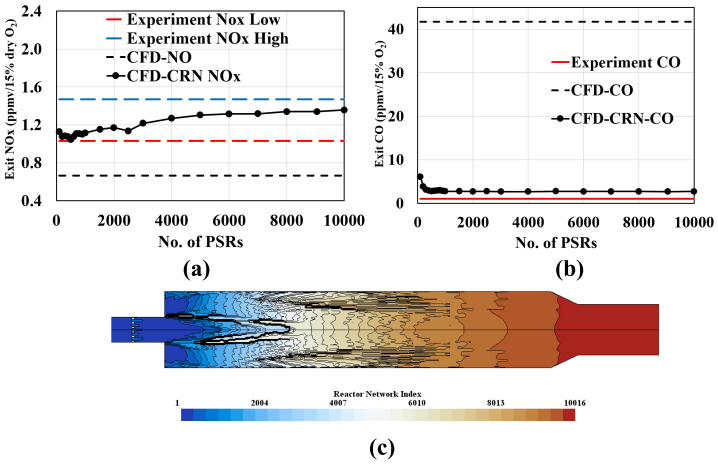

FIGURE 4: (A) EXIT NO_x ($NO + NO_2$) AND (B) EXIT CO PREDICTIONS WITH NUMBERS OF PSR IN REACTOR NETWORK STUDY FOR ϕ =0.5, 100% METHANE-AIR MIXTURE,(C) DISTRIBUTION OF 10000 REACTORS BY REACTOR NETWORK INDEXES

Simcenter STAR-CCM+ using detailed GRI 3.0 chemical kinetic mechanism [26]. The CRNs are created for each pure methane and H_2 enriched methane air cases, using finite intervals for three CFD flow field parameters: temperature (T), equivalence ratio (ϕ), and axial velocity (v_x). Hence, it is important that CFD results should be as realistic as possible especially for temperature, velocity and fuel distribution in order to accurately capture emissions from CRN. The temperature and equivalence ratio as clustering parameter leads to the creation of multiple PSRs in the flame front zone. The axial velocity as clustering parameter can also be used to separate recirculation zones from the flame front into different PSRs. The finite interval of parameters to create homogeneous clusters of cells are used for automatic CRN creation for all the cases. The maximum number for PSRs tested for pure methane cases are up to 10,000, and for cases with H_2 addition are up to 20,000.

In order to decide the sufficient number of PSRs to predict

TABLE 2: PARAMETERS FOR CRN MODELLING (PURE METHANE - AIR MIXTURE)

ϕ	PSRs	Parameters
0.43	5000	$\Delta T = 5\%$, $\Delta V_x = 5\%$, $\Delta\phi = 0.1\%$
0.46	10000	$\Delta T = 1\%$, $\Delta V_x = 2\%$, $\Delta\phi = 2\%$
0.50	10000	$\Delta T = 1\%$, $\Delta V_x = 2\%$, $\Delta\phi = 2\%$
0.53	10000	$\Delta T = 2\%$, $\Delta V_x = 2\%$, $\Delta\phi = 2\%$
0.55	10000	$\Delta T = 2\%$, $\Delta V_x = 2\%$, $\Delta\phi = 2\%$

TABLE 3: PARAMETERS FOR CRN MODELLING (HYDROGEN ENRICHED METHANE - AIR MIXTURE)

$\%CH_4$:$\%H_2$	PSRs	Parameters
$\phi = 0.43$		
90:10	20000	$\Delta T = 1\%$, $\Delta V_x = 2\%$, $\Delta\phi = 2.0\%$
80:20	10000	$\Delta T = 2\%$, $\Delta V_x = 2\%$, $\Delta\phi = 0.1\%$
70:30	10000	$\Delta T = 2\%$, $\Delta V_x = 2\%$, $\Delta\phi = 0.1\%$
60:40	10000	$\Delta T = 2\%$, $\Delta V_x = 2\%$, $\Delta\phi = 0.1\%$
$\phi = 0.50$		
90:10	3000	$\Delta T = 1\%$, $\Delta V_x = 5\%$, $\Delta\phi = 5\%$
80:20	10000	$\Delta T = 1\%$, $\Delta V_x = 2\%$, $\Delta\phi = 2\%$
70:30	20000	$\Delta T = 1\%$, $\Delta V_x = 2\%$, $\Delta\phi = 0.1\%$
60:40	20000	$\Delta T = 2\%$, $\Delta V_x = 2\%$, $\Delta\phi = 0.1\%$

emissions, CRN size independence study have been performed in each case. Figure 4 shows the CRN size independence study for equivalence ratio $\phi = 0.50$ case, where the exit NO_x and CO variation (ppm vol. corrected for dry 15% O_2) are plotted (Fig. 4a and 4b) with number of PSR reactors in the reactor network. Figure 4a also shows the thermal NO predicted at exit by thermal NO modelling in tabulated CFD (dashed black line) and range of measured NO_x at exit from experiments [12] (by red / blue dashed line for low and high values, respectively). The CFD thermal NO predictions are always found to be under-predicted for all the CFD cases studied. Similarly, the experimentally measured CO at exit [12] (with red line) and the over-predicted CO at the exit from the tabulated CFD (dashed blue line) are also plotted in Fig. 4b. It can be observed from Fig. 4a, that the exit NO_x computed from CFD-CRN fluctuates initially as number of PSRs are increased, but after 5000 PSRs and at 10000 PSRs it is almost stable. Similarly, in Fig. 4b, exit CO will become stable even after 500 PSRs in pure methane case at $\phi = 0.5$. Although the exit NO_x predicted by the reactor network is within the experimental range, exit CO is slightly over predicted, compared to the experimental value, but better than high over prediction by CFD. In the case of pure methane (100% CH_4) in premixed methane-air mixture, the reactor network size independence study leads to same number of PSRs as 10000 for all the equivalence ratios, except for $\phi = 0.43$. The parameters of clustering and number of PSR are listed in Table 2. The percentage interval of clustering parameter represents the relative interval with respect to maxima and minima of the parameter in domain. Figure 4c shows the distribution of reactor networks in the combustion domain for pure methane at $\phi = 0.5$ with 10000 PSRs. However, with H_2 addition, it was required to

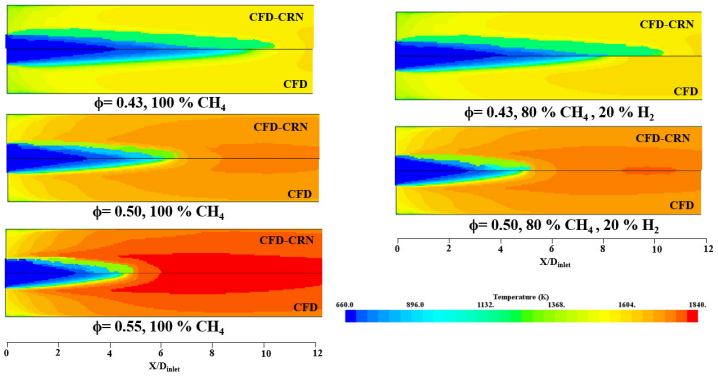

FIGURE 5: CFD AND CFD-CRN TEMPERATURE CONTOUR COMPARISON FOR PURE METHANE (LEFT, ϕ = 0.43, 0.50 AND 0.55) AND 20% H_2 ADDITION (RIGHT, ϕ = 0.43 AND 0.5).

use up to 20000 PSRs to predict the exit NO_x and CO, independent of number of reactors. Table 3 shows various numbers of PSR and clustering parameters for cases with H_2 addition up to 40%. The current version of Simcenter STAR-CCM+ 2019.2, reactor network module does not solve the energy equation. Since, it uses the fast ODE solver CVODE [19], the reactor network solver computes quickly within 0.25 hours for 10000 PSRs (on Intel i7, 3.2 GHz CPU with 32 GB RAM in parallel simulation).

Figure 5 shows the temperature contours from CFD and CFD-CRN studies for different equivalence ratios of pure methane-air mixture as well as for 20% H_2 addition for equivalence ratios ϕ = 0.43 and 0.50. Among the studied equivalence ratios for pure methane-air mixtures, higher equivalence ratio shows higher flame temperature and shorter flame length, while leaner equivalence ratio shows lower flame temperature with longer flame length in CFD. With H_2 addition, it can be seen that the flame length will be slightly reduced in comparison to pure methane cases and the flame temperature have slightly increased with H_2 addition because of higher reactivity of H_2. CFD-CRN predicts the similar temperature profile with 5000 PSRs for equivalence ratios ϕ = 0.43, and 10000 PSRs for ϕ = 0.50, 0.55 of pure methane-air mixture and 20% H_2 addition also for ϕ = 0.43 and 0.50 with 10000 PSRs. However, closer look in the contour profile shows some homogeneous patches in temperature for CFD-CRN, which was expected as the reactor networks model is created from large computation grid to clustered cells of homogeneous zones. Figure 6a shows the comparison between the NO_x ($NO + NO_2$) predicted at the exit by CFD-CRN method for pure methane (100%)-air premixed mixture for five equivalence ratios and the measured experimental exit NO_x[12] (up to ϕ = 0.53). The thermal NO predicted by only CFD also have been plotted along with these predictions. Further, Fig. 6b shows the exit CO predictions by CFD-CRN and compared with the experimental measurements of exit CO [12] (up to ϕ = 0.53). Again, CFD predictions of exit CO based on FGM table have also been plotted here. Figure 6a shows that increase in equivalence ratio from ϕ =0.43 to 0.55 leads to exponential increase in CFD-CRN predicted exit NO_x. CFD predictions with tabulated FGM method and thermal NO modelling are always lower than

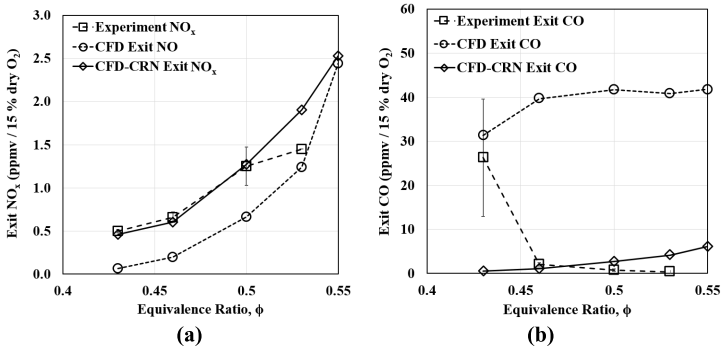

FIGURE 6: CFD-CRN (A) EXIT NO_x (B) EXIT CO PREDICTIONS FOR PURE METHANE (100%)-AIR MIXTURE, COMPARISON WITH EXPERIMENTAL RESULTS AND CFD ONLY PREDICTION

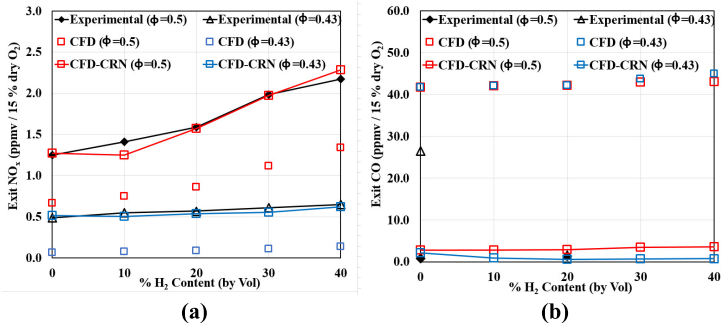

FIGURE 7: EFFECT OF H_2 ADDITION ON (A) EXIT NO_x (B) EXIT CO CFD-CRN PREDICTIONS AT ϕ = 0.43 AND 0.50 UP TO 40% H_2 BY VOLUME

the experimental measurements. CFD-CRN predictions with detailed chemical kinetic mechanism GRI3.0 matches closely for three equivalence ratios ϕ = 0.43, 0.46 and 0.50, while slightly deviates for ϕ = 0.53 than the experimental measurements. For ϕ = 0.55, experimental data is not available, however, CFD-CRN predictions of exit NO_x follows the same exponential trend. The experimental exit CO measurements in Fig 6b for all the equivalence ratios are lower than 1 ppmv (corrected for dry 15% O_2) except for lean mixture of ϕ = 0.43 and it reduces with increase in equivalence ratio. However, CFD prediction with DRM22 mechanism and tabulated chemistry shows high over predictions of exit CO, and opposite trend than the experimental measurements as it slightly increases with increase in equivalence ratios. The prediction from CFD-CRN method with detailed chemical kinetic mechanism GRI3.0 are close to experimental values, except ϕ =0.43 but the trend is similar to CFD predictions. The reason for the measured values of exit CO to be different than the predicted value can be because this equivalence ratio ϕ =0.43, is close to lean blowout limit for pure methane-air mixture, in experiments, there might be high unsteady effects, which reflects in wide range of measured values.

Figure 7 shows the effect of hydrogen addition up to 40% by volume to the methane-air mixture at two equivalence ratios ϕ = 0.43 and 0.50 on exit NO_x and CO predictions by CFD-CRN method. At both equivalence ratios ϕ = 0.43 and 0.50, CFD predictions of thermal NO modelling are almost 40% lower than the experimental measurements for all 10% to 40% H_2 additions. CFD-CRN predictions of exit NO_x matches closely with experimental measurements at both equivalence ratios. However, there is slight deviation less than 4% for 10% H_2 addition for ϕ = 0.50. Exit CO estimations are again highly over-predicted from the tabulated CFD simulations for all the cases. CFD-CRN predictions of exit CO are close to experimental values, except for pure methane at ϕ = 0.43. The above results shows that the CFD-CRN approach can predict the exit NO_x well for range of lean equivalence ratios as well as for H_2 addition up to 40%. However, exit CO predictions are somewhat close to experiments, but do not follow the same trend as experiments. To have exit CO prediction close to experiments, two approaches in future study can be utilized: 1) test of different detailed kinetic mechanism or 2) develop CFD-CRN method based on unsteady CFD simulations.

4.3 NO_x Formation Pathways

The reactor network solution can be further utilized to analyze the NO_x formation pathways in various regions of combustors. Usually, NO_x (NO+ NO_2) can be formed via different chemical routes: (1) Thermal (Zel'dovich) NO (2) Prompt (Fenimore), (3) N_2O Intermediate, (4) Oxidation of NO to NO_2 (5) formation of NNH and (6) fuel bound Nitrogen [4]. In this study, the fuel is either pure methane or H_2 enriched methane, hence, fuel bound nitrogen pathway is not active. Further, GRI 3.0 mechanism [26] is used to compute the chemical reactor network with full NO_x chemistry as well as different separate pathway chemistry by switching off important reactions for first five pathways as mentioned above according to [4]. The next subsections will discuss about NO_x formation pathways at the exit as well as in combustor zones.

4.3.1 Exit NO_x Formation Pathways. Figure 8a shows the exit NO_x formation in ppm by volume, adjusted to 15% dry O_2 for pure methane-air mixture at different equivalence ratios w.r.t. different NO_x formation pathways. The total absolute values of exit NO_x are increasing with increase in equivalence ratio. The percentage contribution of NO_x formation from various pathways are plotted in Fig. 8b. The main contribution of NO_x formation comes from thermal and nitrous oxide N_2O intermediate pathways for pure methane-air premixed mixture. It can be seen that the NO_x formation by the thermal route increases from 5% to 35% with increase in equivalence ratio from ϕ = 0.43 to 0.55 because of increase in flame temperature for higher equivalence ratios. The N_2O intermediate is prevalent in all the conditions because the combustor is operating at high pressure of 5 bar and N_2O pathway is promoted because of third body reaction at high pressure. It is observed that although the percentage contribution of N_2O pathway is reducing with increase in equivalence ratio, the absolute values of NO_x formation through N_2O pathway is increasing with increase in equivalence ratio. It should also be noted that NO_x formation by prompt and NNH pathways increases with increase in equivalence ratio. However, in terms of percentage contribution, there is no significant change. The CFD prediction of exit NO was based on thermal NO modelling,

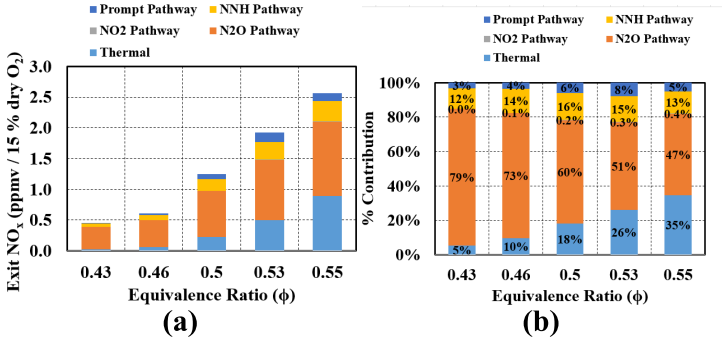

FIGURE 8: EXIT NO_x PATHWAY PREDICTION (A) ABSOLUTE VALUE (B) % CONTRIBUTION FROM EACH PATHWAY FOR 100% METHANE-AIR MIXTURE

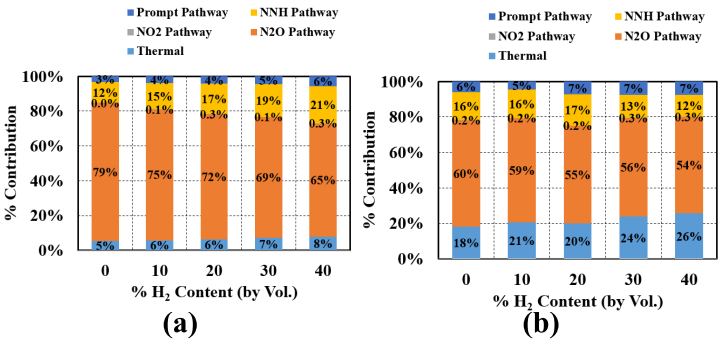

FIGURE 9: EXIT NO_x PATHWAY % CONTRIBUTION (A) ϕ = 0.43 (B) ϕ = 0.50, WITH H_2 ADDITION

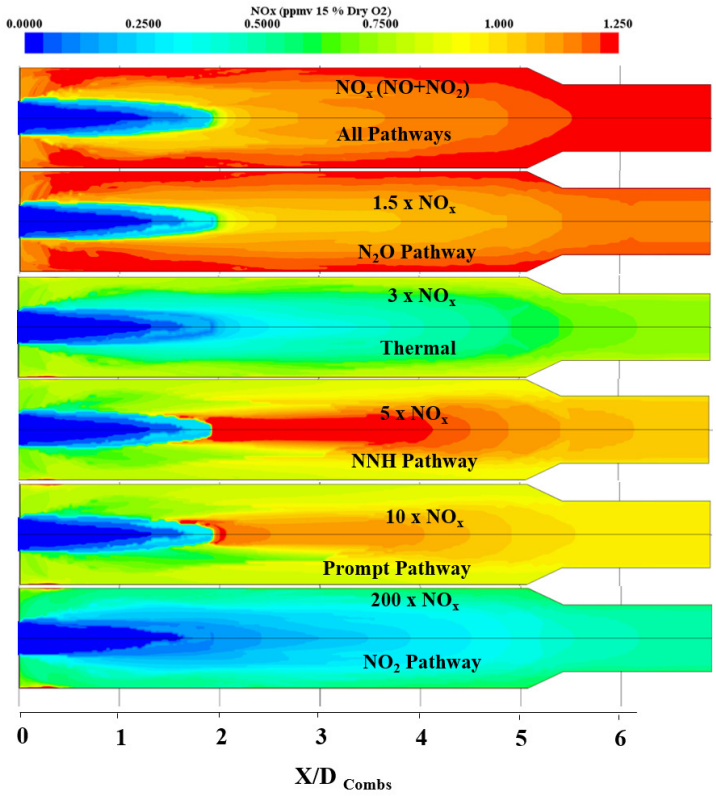

FIGURE 10: DETAILED NO_x FORMATION FROM DIFFERENT PATHWAYS AT ϕ =0.50 WITH 100% METHANE AIR MIXTURE

while CFD-CRN prediction of NO_x is chemical kinetically controlled. The differences in thermal pathway contribution of NO_x from CFD-CRN and CFD predicted thermal NO is because of difference in prediction methods. However, it is observed that CFD predicted thermal NO is always lesser than thermal NO_x contribution from CFD-CRN.

Figure 9 shows the exit NO_x formation contribution by different chemical routes for H_2 addition at two equivalence ratios ϕ = 0.43 to 0.50. In case of leaner equivalence ratio (ϕ = 0.43), the percentage contribution of N_2O pathway decreases from 79% to 65%, with increase in H_2 content. However, there is slight increase in percentage contribution from thermal pathway as the flame temperature increases 5~ 10 K with increase in H_2 content. The NNH pathway contribution increases from 12% to 21% for leaner equivalence ratio with increase in H_2 content. The reason for this may be because there will be higher availability of O_2 and oxygen atoms, with increase in H_2 content in mixture, that can facilitate, oxidation of short-lived N_iH_j to NO. In case of equivalence ratio ϕ = 0.50, there is not significant changes in percentage contribution from NNH Pathway and Prompt pathway with H_2 increase. Because of slight increase in flame temperature, the thermal route contribute slightly higher in NO_x formation and proportionally there is decrease in contribution from (N_2O) pathway. It can be concluded here, that H_2 addition at lean condition may lead to higher increase in NNH pathway of NO_x formation.

4.3.2 NO_x Formation Pathways in Combustor. The CRN study with large number of reactors is motivated because of its potential to understand the details of emission formation in various zones of real combustor e.g. pre-heat, flame-zone or post-flame zones, recirculation zones. In this section, NO_x formation in the combustor domain have been studied. Figure 10 shows the z-plane section of combustor with NO_x formation (in ppmv /15% dry O_2) from different pathways for equivalence ratio ϕ =0.50 of 100% methane-air mixture. Further, Fig. 11 shows the NO_x formation along the combustor axis (left) and radial direction (right) across the flame (at location 75 mm from the dump inlet) for three equivalence ratios (ϕ = 0.43, 0.50 and 0.55). In Fig 10, all the individual pathways scaled up to clearly visualize the NO_x variations. As mentioned earlier that in the high pressure combustor, the main contribution of NO_x formation comes from thermal pathway and nitrous oxide (N_2O) intermediate pathways for lean mixtures of pure methane. At lean mixtures, N_2O pathway is promoted in the regions of high pressure because it initiates from third body reaction. In this study at equivalence ratio ϕ =0.50, the maximum contribution comes from N_2O intermediate pathway in the post flame and recirculation regions. The thermal pathway contributed in high temperature zones. Further NNH pathway contribution is higher in axial direction of post-flame. And prompt pathway contributes maximum in the flame thickness zone. There is almost negligible contribution from NO_2 pathway. Figure 11b, shows axial variation of NO_x from the different pathways. In the near post flame zone, the contribution of NNH

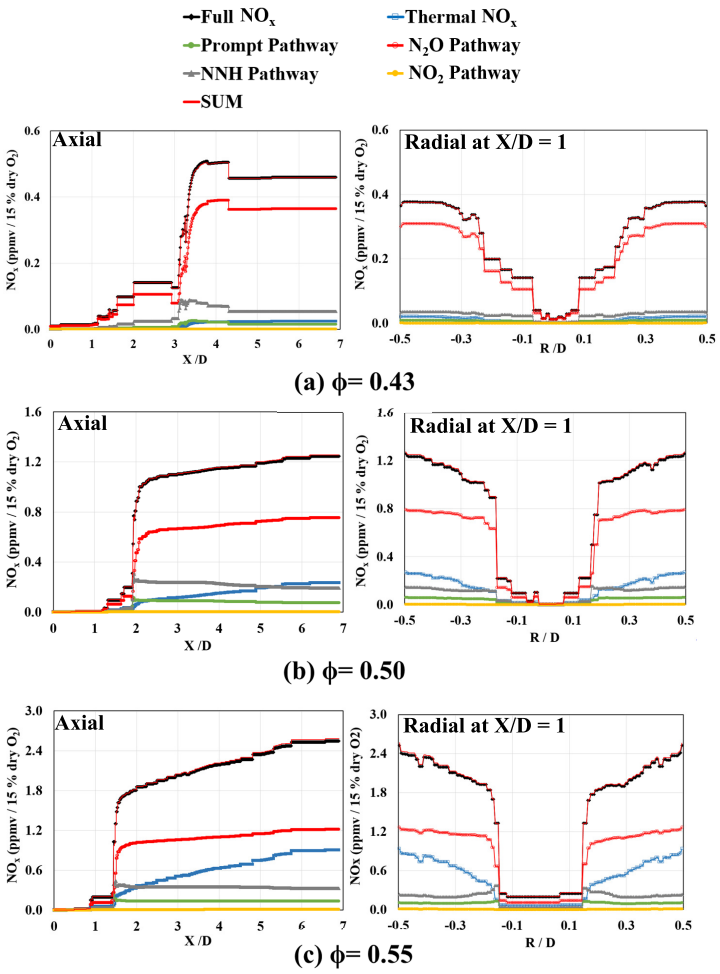

FIGURE 11: NO_x VARIATION ALONG THE AXIS (LEFT) AND RADIAL DIRECTION (AT X/D_{combs} = 1) WITH DIFFERENT PATHWAYS FOR PURE METHANE-AIR MIXTURE

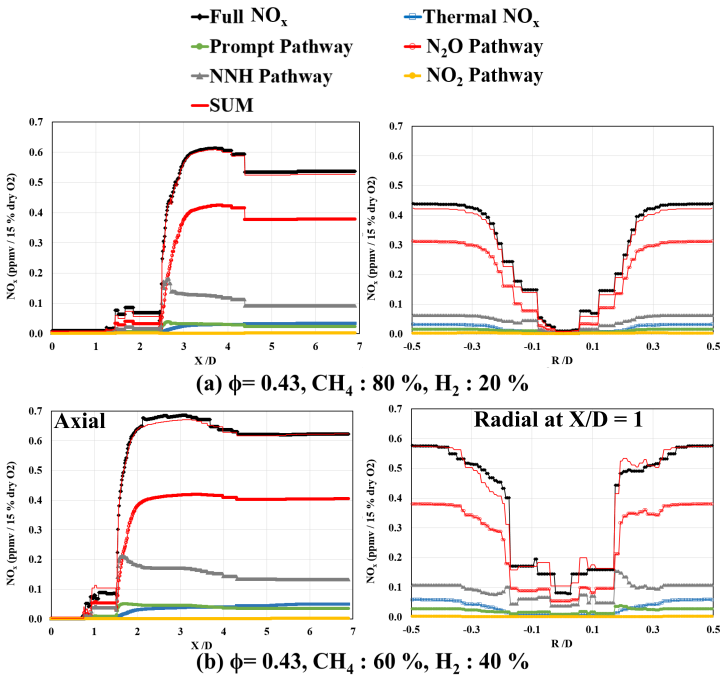

FIGURE 12: NO_x VARIATION ALONG THE AXIS (LEFT) AND RADIAL DIRECTION (AT X/D_{combs} = 1) WITH DIFFERENT PATHWAYS FOR ϕ = 0.43 WITH 20% AND 40% H_2 CONTENTS BY VOLUME

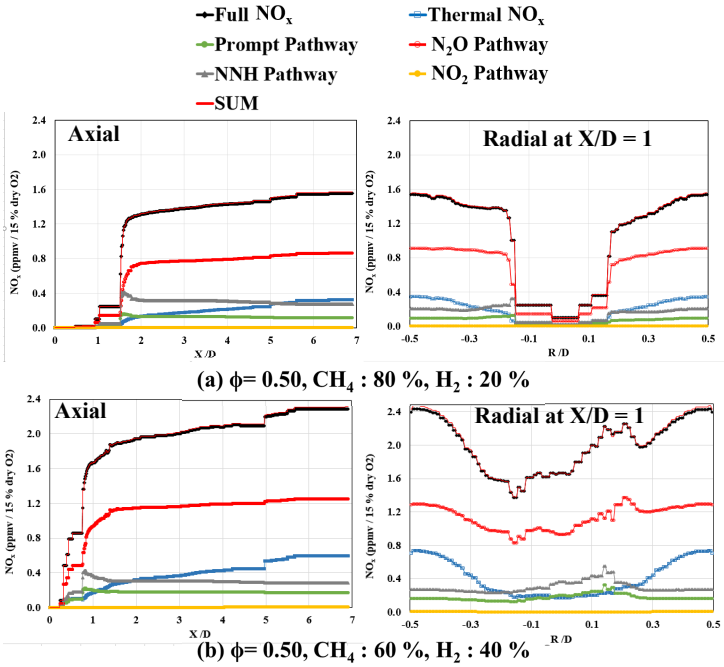

FIGURE 13: NO_x VARIATION ALONG THE AXIS (LEFT) AND RADIAL DIRECTION (AT X/D_{combs} = 1) WITH DIFFERENT PATHWAYS FOR ϕ = 0.50 WITH 20% AND 40% H_2 CONTENTS BY VOLUME

pathway is higher than the thermal pathway. However, across the flame in radial image, the thermal pathway contributes more than the NNH pathway.It is to note that in Fig. 11 the Y-scales are different for all three equivalence ratios. But for the lean mixture of pure methane-air (ϕ = 0.43), the contribution from N_2O intermediate is higher than other pathways in pre-heat zone and post flame zone. The contribution from NNH pathway is also higher than the thermal pathway because of comparatively low flame temperature in the combustor. Similarly across the flame in radial image, N_2O contribution is way higher than other pathways. As the flame temperature increases in ϕ = 0.55 case, the contribution from thermal pathway reaches closer to N_2O pathway NO_x formation along the axis as well as across the flame. The crossing of Thermal pathway NO_x production to NNH pathway occur closer to the flame as equivalence ratio increases.

Figure 12 and 13 show the NO_x formation through different pathways along the axis of combustor and in radial direction at 75 mm from dump inlet for 20% and 40% H_2 addition at two equivalence ratios, ϕ = 0.43 and 0.50, respectively. In Fig. 12a and b, as the H_2 content increases at lean equivalence ratio, ϕ = 0.43, the NNH pathway NO_x formation increases than compare to pure methane case (Fig. 11a). Further as the flame become shorter (213

mm with pure CH_4 and 106 mm with 40% H_2 addition, across the flame also in radial profile, the NO_x formation become higher near the flame zone. With H_2 addition there are significant increase in NO_x formation through NNH pathway. Figure 13a and b show NO_x variation with 20% and 40% H_2 addition at equivalence ratio ϕ = 0.50. At this equivalence ratio, with increase in H_2, the flame length significantly reduces from 138 mm to 50 mm as well as flame temperature also increases slightly up to 5 ~ 10 K at each 10% H_2 increase. The thermal and N_2O intermediate NO_x formation increases with increase in H_2 content, causes overall slight increase in NO_x emission. However, the NO_x formation because of NNH pathway does not change significantly as it was contributing at leaner equivalence ratio.

5. CONCLUSION

In the current study, hybrid CFD-CRN method has been used in single framework of Simcenter STAR-CCM+ 2019.2. Combustion modelling is performed by FGM model in CFD along with all three heat transfer modes. The exit temperatures and flame front locations have been compared with experimental data for five pure methane equivalence ratios as well as H_2 enriched methane-air flames at two equivalence ratios. With adequate accuracy of CFD simulations, reactor network modelling is performed for all the cases by using automated clustering algorithm based on temperature, equivalence ratio and axial velocity. The reactor networks are solved using PSRs; and CRN size independence study have been performed for each test case. Pure methane-air mixtures require up to 10000 PSRs to accurately predict exit NO_x, however for H_2 enriched methane-air mixture, larger CRN networks up to 20,000 PSRs are required. The CRN solver in Simcenter STAR-CCM+ has been found advantageous in solving large reactor networks with lesser computation time e.g. 10000 PSRs can be solved as quick as 0.25 hour on a standard Intel i7 desktop. Exit NO_x have been predicted close to experimental data for all the case using CFD-CRN, while exit CO have been predicted closer to experimental data, but have opposite trend than experimental trend with increase in equivalence ratio, this trend is similar to CFD CO predictions. The detailed NO_x pathways study give insight of NO_x formation in pure and H_2 enriched methane-air flame. In pure methane-air lean mixture at ϕ = 0.43, the N_2O intermediate pathway significantly contribute to NO_x formation. As the equivalence ratio increases, the N_2O pathway contribution reduces as thermal contribution increases. Other pathways prompt, NNH and NO_2 does not change or contribute significantly. The effect of increase in H_2 content in the mixture have different effect on different equivalence ratio. At lean equivalence ratio (ϕ = 0.43), increase in H_2 content leads to increase in NNH pathway percentage contribution and reduction in N_2O pathway contribution. At equivalence ratio ϕ = 0.50, there is small increase in thermal pathway, while proportional decrease in N_2O intermediate pathway.

To conclude, the reactor network module in current version of Simcener STAR-CCM+ 2019.02 have advanges of: 1) solving and postprocessing CFD and CRN hybrid study in the same framework, 2) automatically construction the reactor networks using clustering algorithm on large domains 3) it can solve large reactor network quickly by using efficient ODE integration of CVODE solver. However, further enhancement in the later versions addressing followings can be very useful for future studies: 1) The CRN solver does not solve energy equation, 2) there is no option to generate reactor network from time-averaged URANS or LES data.

PERMISSION OF USE

ACKNOWLEDGEMENT

The authors wish to acknowledge funding support from Siemens Canada Limited and Science Foundation Ireland through the SEFE Spoke of the MaREI Research Centre for Marine and Renewable Energy in Ireland (Grant 16/SP/3829). In addition, the authors would like to acknowledge support of Siemens-PLM for providing Simcenter STAR-CCM+ 2019.2 version with reactor network capability.

REFERENCES

[1] Yousefian, S., Bourque, G., and Monaghan, R. F. D., 2017, "Review of Hybrid Emissions Prediction Tools and Uncertainty Quantification Methods for Gas Turbine Combustion Systems", Proceedings of the ASME Turbo Expo 2017: Turbomachinery Technical Conference and Exposition. Volume 4B: Combustion, Fuels and Emissions. Charlotte, North Carolina, USA. June 26–30, 2017. doi:10.1115/GT2017-64271.

[2] Ehrhardt KR., 1993, "Development of a hybrid model for the prediction of nitric oxides emissions of furnaces", Energy Lab. Report. Boston, USA: M.I.T.

[3] Ehrhardt K., Tokan M., Jansohn P., Teare J.D., Ber J.M., Sybon G., Leuckel W., 1998, "Modeling of NO_x reburning in a pilot scale furnace using detailed reaction kinetics. Combust Science & Technology, 136:333–47. doi:10.1080/00102209808935758.

[4] Monaghan, R. F. D., Tahir, R., Cuoci, A., Bourque, G., Furi, M., Gordon, R. L., Faravelli, T., Frassoldati, A., and Curran, H. J., 2012, "Detailed multi-dimensional study of pollutant formation in a methane diffusion flame," Energy and Fuels, 26(3), pp. 1598–1611. doi:10.1021/ef300515q.

[5] Monaghan, R. F. D., Tahir, R., Bourque, G., Gordon, R. L., Cuoci, A., Faravelli, T., Frassoldati, A., and Curran, H. J., 2014, "Detailed emissions prediction for a turbulent swirling non premixed flame," Energy and Fuels, 28(2), pp. 1470–1488.doi:10.1021/ef402057w.

[6] Yousefian, S., Bourque, G., Monaghan, R.F.D., "Uncertainty Quantification of NO_x Emission Due To Operating Conditions and Chemical Kinetic Parameters in a Premixed Burner". ASME J. Eng. Gas Turbines Power 2018;140:121005-1–11. doi:10.1115/1.4040897.

[7] Yousefian, S., Bourque, G., Monaghan, R.F.D., "Uncertainty quantification of NO_x and CO emissions in

a swirl-stabilized burner“. J. Eng Gas Turbines Power 2019;141:101014-1–13. doi:10.1115/1.4044204.

[8] Fichet, V., Kanniche, M., Plion, P., and Gicquel, O., 2010, “A reactor network model for predicting NO_x emissions in gas turbines,” Fuel, 89(9), pp. 2202–2210. doi:10.1016/j.fuel.2010.02.010.

[9] Cuoci, A., Frassoldati, A., Buzzi Ferraris, G., Faravelli, T., and Ranzi, E., 2007, “The ignition, combustion and flame structure of carbon monoxide/hydrogen mixtures. Note 2: Fluid dynamics and kinetic aspects of syngas combustion,” Int. J. Hydrogen Energy, 32 (15 SPEC. ISS.), pp. 3486–3500. doi:10.1016/j.ijhydene.2007.02.026.

[10] Stagni, A., Cuoci, A., Frassoldati, A., Faravelli, T., and Ranzi, E., 2014, “A fully coupled, parallel approach for the post-processing of CFD data through reactor network analysys, ” Comp. Chem. Eng., 60, pp. 197-212. doi:10.1016/j.compchemeng.2013.09.002.

[11] STAR-CCM+ User Guide, Ver. 2019.2; Siemens PLM: 2019.

[12] Boschek E., Griebel, P., Jansohn P., “Fuel variability effects on turbulent, lean premixed flames at high pressures”, Proceedings of the ASME Turbo Expo 2007: Power for Land, Sea, and Air. Volume 2: Turbo Expo 2007. Montreal, Canada. May 14–17, 2007. pp. 373-382. ASME. doi:10.1115/GT2007-27496.

[13] Griebel P., Boschek E., Jansohn P., “Lean Blowout Limits and NO_x Emissions of Turbulent, Lean Premixed, Hydrogen-Enriched Methane/Air Flames at High Pressure”, 2007, J. Eng. Gas Turbines Power, 129(2): 404-410. doi:10.1115/1.2436568.

[14] Siewert, P., “Flame front characteristics of turbulent lean premixed methane / air flames at high-pressure”, Doctoral Thesis, ETH Zurich, 2006.

[15] Lieuwen T.C.,Chang M., Amato A., “Stationary gas turbine combustion: Technology needs and policy considerations”, Combustion Flame 160 (8) (2013)1311–1540, doi:10.1016/j.combustflame.2013.05.001.

[16] Taamallah S. ,Vogiatzaki K., Alzahrani F.M., Mokheimer E.M.A., Habib M.A.,Ghoniem A.F., 2015, “Fuel flexibility, stability and emissions in premixed hydrogen-rich gas turbine combustion: Technology, fundamentals, and numerical simulations”, Applied Energy 154: 1020-1047. doi:10.1016/j.apenergy.2015.04.044.

[17] Rajpara P., Shah R., Banerjee J., 2018, “Effect of Hydrogen addition on combustion and emission characteristics of methane fuelled upward swirl can combustor”, International Journal of Hydrogen Energy, Vol. 43, Issue 36, 17505-17519. doi:10.1016/j.ijhydene.2018.07.111.

[18] de Persis S., Idir M., Molet J.,Pillier L., 2019,“Effect of Hydrogen addition on NO_x formation in high-pressure counter flow premixed CH_4/air flames”, International Journal of Hydrogen Energy, Vol. 44, Issue 41, 23484-23502. doi:10.1016/j.ijhydene.2019.07.002.

[19] Cohen, S. D., and Hindmarsh, A. C., “CVODE, a stiff/nonstiff ODEsolver in C”, Computers in Physics 10, 2 (March-April 1996), 138–143. doi:10.1063/1.4822377.

[20] Griebel P., Siewert P. and Jansohn P., “Flame characteristics of turbulent leanpremixed methane/air flames at high pressure: Turbulent flame speed and flame brush thickness”, Proceedings of the Combustion Institute 31 (2007) 3083–3900. doi:10.1016/j.proci.2006.07.042.

[21] Kazakov, A., and Frenklach, M.,“Reduced Reaction Sets based on GRI-Mech 1.2” accessed on Jan 2020, http://combustion.berkeley.edu/drm/drm22.dat.

[22] Dinkelacker, F., Manickam, B., Muppala, S.P.R., “Modelling and simulation of lean premixed turbulent methane/hydrogen/air flames with an effective Lewis number approach”, Combustion and Flame 158 (2011) 1742–1749. doi:10.1016/j.combustflame.2010.12.003.

[23] Lyra, S., Cant, R.S., “Analysis of high pressure premixed flames using Equivalent Reactor Networks for predicting NO_x emissions”,Fuel 107 (2013) 261–268. doi:10.1016/j.fuel.2012.12.066.

[24] Sergeev, O., Shashkov, A., Umanskii, A., “Thermophysical properties of quartz glass”, Journal of Engineering Physics 43, 1375–1383 (1982). doi:10.1007/BF00824797.

[25] Grosshandler, W.L., 1993, “RADCAL: A narrow band model for Radiation Calculations in a Combustion Environment”, NIST Technical Note 1402, accessed on Jan 2020 https://www.sandia.gov/TNF/radiation.html.

[26] Gregory P. Smith, David M. Golden, Michael Frenklach, Nigel W. Moriarty, Boris Eiteneer, Mikhail Goldenberg, C. Thomas Bowman, Ronald K. Hanson, Soonho Song, William C. Gardiner, Jr., Vitali V. Lissianski, and Zhiwei Qin, “GRI-MECH 3.0”, last accessed on Jan. 2020, http://combustion.berkeley.edu/gri-mech/releases.html.